2021

Physicochemical implications of cyanobacteria oxidation with Fe(VI)

Erika L. Addison

Kyle T. Gerlach

Charles D. Spellman Jr.

Grace Santilli

Alyson R. Fairbrother

See next page for additional authors

Authors

Erika L. Addison, Kyle T. Gerlach, Charles D. Spellman Jr., Grace Santilli, Alyson R. Fairbrother, Zachary Shepard, Jeanine D. Dudle, and Joseph E. Goodwill

Physicochemical implications of cyanobacteria oxidation with Fe(VI)

Erika L. Addison[a], Kyle T. Gerlach[b], Charles D. Spellman Jr.[a], Grace Santilli[a], Alyson R. Fairbrother[a,c], Zachary Shepard[a], Jeanine D. Dudle[b], Joseph E. Goodwill[a]*

[a]Department of Civil and Environmental Engineering,
University of Rhode Island, Kingston, RI 02881 USA
[b]Department of Civil and Environmental Engineering,
Worcester Polytechnic Institute, Worcester, MA 01609 USA
[c]Tighe & Bond
300 West Exchange Street, Providence, RI 02903 USA
*Corresponding author.
E-mail address: goodwill@uri.edu (J.E. Goodwill)

Abstract

Increases in harmful algal blooms has negatively impacted many surface-sourced drinking water utilities. To control these blooms, many water utilities implement pre-oxidation with ozone, chlorine, or permanganate; however, pre-oxidation of algae has both positive and negative water quality outcomes. This study investigated ferrate (Fe(VI)) as an alternative oxidant by measuring its effect on cell lysing, surface characteristics, and coagulation in waters containing the cyanobacteria *Microcystis aeruginosa*. Bench scale studies were conducted to examine the complex combination of processes in a Fe(VI)-algae system. These processes were characterized by fluorescence index, surface charge, collision frequency modeling, particle counts and sphericity, total nitrogen, and ferrate decomposition measurements. Results showed that Fe(VI) lysed algal cells, but further oxidation of released organic matter is possible. The presence of algae did not significantly impact the rate of Fe(VI) decomposition. Fe(VI) pre-oxidation may also be capable of decreasing the formation of nitrogenated disinfection byproducts through subsequent oxidation of released nitrogen rich organic matter. Streaming current and zeta potential results indicate destabilization of the resulting algae and iron suspension was incomplete under most conditions. Particle collision frequency modeling indicates fluid shear to be an important aggregation mechanism of the resulting suspension. Overall, Fe(VI) is a viable alternative to other strong oxidants for water utilities struggling with harmful algal blooms, but the final fate of the resulting organic matter must be further studied.

Keywords: Harmful Algae Bloom; Microcystis aeruginosa; Ferrate; Fe(VI); Oxidation; Coagulation

1. Introduction

Algal blooms in surface waters are a major threat to water quality and public health, especially when the surface waters are sources of drinking water (Brooks et al., 2016). The occurrence of harmful algal blooms (HABs) are expected to increase as global water temperatures increase (Paerl and Huisman, 2008), and occur in areas that historically have not had HAB problems. In some situations, an increase in

algae may also be an unintended consequence of successful acid rain mitigation that has increased pH to levels more conducive to the autochthonous production of organic carbon (Anderson et al., 2017).

Microcystis aeruginosa is a common type of cyanobacteria (e.g. blue-green algae) that occurs in fresh and brackish waters (Codd et al., 1989). In general, individual *M. aeruginosa* cells are polydisperse, ranging in diameters from 3 to 10 μm (Dang et al., 2012; Fang et al., 2010; Li et al., 2016; Vlaski, 1998). This cyanobacteria species is also toxin-producing, and can cause serious liver, digestive, neurological, and skin issues in humans (Kenefick et al., 1993). Therefore, it is imperative to find the best practices to mitigate the impact of *M. aeruginosa* on drinking water supplies.

To control HABs, water utilities can employ several different technologies, including powdered activated carbon adsorption, and oxidation with strong oxidants, like ozone. Ozone is generally effective at addressing algal blooms and associated toxins (Loganathan, 2016). However, ozone generation, contact, and off-gas destruction equipment requires capital investment for permanent infrastructure needed to address algae concerns that are likely episodic and difficult to predict. A similar dilemma confronts other on-site strong oxidant generation approaches (e.g. chlorine dioxide and UV/H_2O_2) Oxidation of HABs with free chlorine is generally effective, but may increase the formation of disinfection byproducts (DBPs) (Xie et al., 2013). Permanganate (MnO_4) is another option (Chen and Yeh, 2005; Ma et al., 2012a); however, health concerns related to the exposure of manganese (Mn), an unavoidable byproduct of permanganate oxidation, exist (Tobiason et al., 2016). These heath concerns have resulted in Mn being placed on the Contaminant Candidate List in the United States with a recommended secondary maximum contaminant limit of 50 μg/L (Bouchard et al., 2018) while Canada has established a regulated maximum acceptable concentration of 120 μg/L. Ultimately, the use and selection of the best strong oxidant for HAB treatment is still unclear (Drikas et al., 2001).

Ferrate (Fe(VI)) is emerging as an alternative oxidant in water treatment due to its strong oxidation potential and limited production of hazardous by-products (DeLuca et al., 1983; Gan et al., 2015; Jiang et al., 2019; Sharma et al., 2016). Fe(VI) may be generated onsite as a liquid sodium ferrate product, or generated off-site and shipped as a stable potassium ferrate (K_2FeO_4) salt (US Patent 8.449,756 B2:

63 Monzyk et al., 2013). The use of ferrate as K_2FeO_4 has low capital expenses and can be utilized as needed
64 to address urgent water quality concerns, making it more conducive to urgent episodic use (Cui et al.,
65 2018).

66 Fe(VI) use does not directly generate a hazardous byproduct such as $KMnO_4$ (i.e. Mn). Furthermore,
67 Fe(VI) does not directly form halogenated DBPs, although formation of bromate has been noted (Huang
68 et al., 2016; Jiang et al., 2016a), with yields lower than similar dosages of ozone (Jiang et al., 2019). In
69 addition, the in-situ formation of Fe(III) particles a γ-Fe_2O_3 core and a γ-FeOOH shell that may benefit
70 downstream treatment processes (Deng et al., 2018; Goodwill et al., 2015; Lv et al., 2018; Prucek et al.,
71 2013) by decreasing the amount of coagulant needed due to the formation of Fe(III) during ferrate
72 decomposition (Jiang et al., 2016b). However, questions about coagulation efficacy and dominant
73 mechanisms remain, with differential settling (e.g. "sweep flocculation") being proposed (Lv et al., 2018).

74 Removal of the toxin microcystins-LR (MC-LR) from the cyanobacteria *Planktothrix* by Fe(VI)
75 oxidation has been analyzed (Yuan et al., 2002). It was found that the toxin was easily decomposed by
76 oxidation, but the removal efficiency depended on Fe(VI) dose, pH, and contact time. The degradation of
77 MC-LR follows second-order kinetics that decreases with increasing pH (Jiang et al., 2014). Similarly,
78 the effect of Fe(VI) pre-oxidation on cell viability of *M. aeruginosa* and the fate of microcystins (MC) in
79 various waters investigated by Fan et al. (2018) found that while Fe(VI) induced cell lysis, there was no
80 significant increases in extracellular MC. A possible mechanism for this may be that reactive oxygen
81 species and H_2O_2 formed during the decomposition of potassium ferrate enter the cells and oxidize
82 intracellular MC (Sharma et al., 2015). Fan et al. (2018) also determined that the effectiveness of Fe(VI)
83 oxidation was decreased by high concentrations of natural organic matter (NOM).

84 The effect of Fe(VI) oxidation and coagulation on *M. aeruginosa* cell integrity, intracellular organic
85 matter (IOM) release, and DBP formation has been observed using flow cytometry (Zhou et al., 2014).
86 IOM release was discovered to increase with ferrate dose, and IOM is known to produce DBPs during
87 subsequent treatment processes. Conversely, Fe(VI)-induced coagulation can destabilize *M. aeruginosa*
88 cells, decrease the amount of algal organic matter (AOM) released, and lower concentrations of THMs

89 and HAAs (Liu et al., 2017; Zhou et al., 2014). Liu and Liang (2008), and Ma and Liu (2002) found that
90 Fe(VI) pre-oxidation improved removal of green algae species with prolonged pretreatment time while
91 also decreasing the required alum dosage for effective coagulation. Lastly, Alshahri et al. (2019) found
92 that ferrate was more effective in removing AOM than $FeCl_3$ in seawater.

93 Prior studies increase understanding of the Fe(VI)-algae system, but also have limitations. Most
94 freshwater studies used waters not demonstrative of drinking water quality, pH values > 8, or cell
95 concentrations in the millions of cells per mL, which is not representative of bloom concentrations that
96 may impart low to moderate adverse health effects (20,000 and 100,000 cells/mL) per World Health
97 Organization guidelines (WHO, 2003). Additionally, the dominant collision mechanism between Fe(VI)
98 resulting particles and *M. aeruginosa* cells has not been examined. The overall goal of this study was to
99 fill research gaps in the use of ferrate for HAB mitigation in realistic bloom algal cell concentrations and
100 other relevant drinking water supply conditions. Specific objectives of the research included: (1)
101 determine the effects and extent of Fe(VI) on algal cell lysing, including IOM and total nitrogen (TN), (2)
102 quantify surface charges on resulting Fe(III)- *M. aeruginosa* suspensions, (3) elucidate dominant
103 mechanisms of collisions between particles, and (4) to explicate corresponding resultant particle size
104 distributions.

105 ## 2. Materials and Methods

106 ### 2.1. Chemicals and Reagents

107 High purity (> 92%) Potassium ferrate (K_2FeO_4) was acquired as a dry, crystalline powder from
108 Element 26 Technology (Friendswood, TX, USA), utilizing an electrochemical production method (US
109 Patent 8.499,756 B2) All other chemicals were purchased from Fisher Scientific (Fair Lawn, NJ, USA),
110 and were reagent grade.

2.2. Algal Culturing and Suspensions

Initial cultures of *Microcystis aeruginosa* were acquired from the University of Texas at Austin Culture Collection of Algae. The cultures were grown in batch mode in autoclaved 250 mL Erlenmeyer flasks containing 5 mL of *M. aeruginosa,* and 145 mL of sterile Bold 3N media made following the method from Plummer & Edzwald (2002). Stock cultures of the *M. aeruginosa* cells in log growth phase (approximately 1,500,000 cells/mL) were collected and separated from the Bold 3N media via centrifugation (Sorvall Legend X1R, Thermo Scientific). Algal cell concentrations of either 20,000 cells/mL or 100,000 cells/mL (± 10%) were used for the experiments, and verified using a laser light blockage particle counter (PC5000, Chemtrac). These algal cell concentrations were chosen based on the WHO guidelines for cell counts that generally indicate a cyanobacterial bloom (WHO, 2003). Additional information on the growth, harvesting, separation, and preparation of algal cultures and suspensions can be found in Text SI-1.

2.3. Ferrate Pre-oxidation Reaction

Ferrate pre-oxidation experiments were carried out in mixed, cubic batch reactors (PB-900 Programmable Jar Tester, Phipps & Bird) at room temperature (20 ± 1°C). The desired concentration of algae (20,000 cells/mL or 100,000 cells/mL) was added to each reactor, along with 1 mM of bicarbonate buffer (HCO_3^-) and reagent grade water (RGW) to reach a total volume of 1 L. The pH of the solution was adjusted to either 6.2 ± 0.1 or 7.5 ± 0.1 by the drop-wise addition of 2% H_2SO_4. After the pH was adjusted, a predetermined dose of ferrate (0, 20, 50, or 100 μM) was added to the beaker and rapidly mixed ($G \approx 150\ s^{-1}$) for 1 minute, followed by slow mixing ($G \approx 55\ s^{-1}$) for 30 minutes when the pH was 6.2, or 60 minutes when the pH was 7.5. The pH was adjusted as necessary during mixing by drop-wise addition of 2% H_2SO_4 or 5% NaOH. Samples were collected for further analyses after slow mixing. Reaction completion (i.e. absence of oxidants) was confirmed by indirectly measuring the resultant Fe(VI) concentration using the ABTS spectrophotometric method (Lee et al., 2005) and no quenching agents were utilized.

2.4. Analytical Methods

2.4.1. Particle Size

Particle size measurements between 2 μm and 125 μm were measured on a laser light blockage (LLB) particle counter (PC5000, Chemtrac). A 1 mL sample taken from the reactor at 2 cm below the water surface was diluted to 1:100, and analyzed. The dilution was made to prevent coincidence errors on the particle counter. For particle size measurements between 10 nm and 10,000 nm, an additional 10 mL sample was taken from the reactors at 2 cm below the water surface and analyzed using a Dynamic Light Scattering (DLS) instrument (Zetasizer Nano ZA, Malvern Instruments). The DLS approach is more appropriate for monodispersed, homogenous solutions with particle sizes below 10 μm, as it is based on particle diffusion. The algal solutions created for the experiments are not monodispersed, and thus the number output from the instrument is an estimate. DLS results are not reported for algae only conditions, as *M. aeruginosa* cells are exclusively > 1 μm (Hadjoudja et al., 2010; Li et al., 2016). The measurement method included 7 replicate measurements, each with 9 runs.

Particle size was also characterized on a mass basis by iron fractionation with several filters of progressively smaller effective size exclusions following the procedure outlined by Goodwill et al. (2015). Total iron was measured using the Hach FerroVer® colorimetric method (10249) with a spectrophotometer (DR1900, Hach), conforming to Standard Methods Section 3500-Fe B (Rice et al., 2012).

2.4.2. Surface Charge

Surface charge of resulting particles were assessed via zeta potential and streaming current measurements. Zeta potential values were measured using the DLS instrument, with an overall approach similar to the particle size measurement method. The DLS technique calculates ZP by optically measuring the electrophoretic mobility of particles smaller than 10 μm. Streaming current measurements were made using a laboratory charge analyzer (LCA-01, Chemtrac) and included cationic polymer (Nalco Nacrolyte) titrations to determine the amount of additional coagulant needed to completely neutralize the surface

charge of the algae-ferrate suspension. The LCA measures the change in conductivity for a wide range of particle sizes by imparting motion to the fluid suspension in order to displace the electrical double layer next to the charged particles. The displacement of the electrical charges creates a current corresponding to the amount of charge on the particles. 500 mL samples were placed into a beaker on a stir plate. The solution was slowly mixed ($G \approx 55\ s^{-1}$), and the initial pH was recorded. The polymer was diluted with RGW just prior to use to achieve a stock concentration of 11.6 mg/mL. Small doses of the coagulant were added over time while the streaming current value (SCV) of the solution was monitored. The final pH of the solution, and the total amount of coagulant added to achieve a SCV of 0 were recorded.

2.4.3. Cell Lysing

Excitation-emission scans were collected on a fluorescence spectrophotometer (LS 55 Fluorescence Spectrophotometer, PerkinElmer) to identify cell lysing (Wert et al., 2014). Samples were first filtered through a 0.2 µm MF and then excited at 370 nm. The fluorescence intensity was measured at emission wavelengths from 300 nm to 800 nm in 2 nm increments, and the excitation and emission monochromator bandpasses were set at 5 nm. Fluorescence index (FI) was calculated as the ratio of emission intensities (470 nm divided by 520 nm) at an excitation wavelength of 370 nm (Cory et al., 2010; McKnight et al., 2001). As a ratio, FI is a concentration-independent metric when applied over a narrow range of concentrations (Wert et al., 2014). Each fluorescent sample was measured in triplicate.

Cell lysing was also quantified via total nitrogen measurements. A full description of the methods and reagents used for the total nitrogen tests can be found in Text SI-2. Cell sphericity and 3-dimensional fluorescence images of algal cells before and after ferrate pre-oxidation as a direct indication for lysing were captured using high-content phenotypic-screening confocal fluorescence microscopy (Opera Phenix High Content Screening System, PerkinElmer). Detailed methods regarding the confocal fluorescence microscope and sphericity calculations can be found in Text SI-3.

2.5. Collision Frequency Modeling

Rectilinear Brownian motion (β_μ), fluid shear (β_M), differential sedimentation (β_{DS}), and total (β_{ij}) collision frequencies as a function of particle size were calculated using particle size distributions (PSDs) collected from the laser light blockage particle counter after ferrate pre-oxidation tests. The volume-average particle diameter (d_i) used as the constant diameter of one of the two particles is defined in Eq. (1):

$$d_i = [\left(\sum n_n d_n\right) / \left(\sum n_n\right)]^{1/3} \quad (1)$$

where n_n is the number of particles in the nth channel of the particle counter, and d_n is the average diameter of the nth channel of the particle counter (Chandrakanth and Amy, 1996).

Two particle densities were used in the collision modeling: 978 kg/m^3 (*M. aeruginosa* at 20°C (Li et al., 2016)) and 1500 kg/m^3 (a relatively high iron-based floc density (Bache and Gregory, 2010)). The rectilinear collision frequency functions are expressed by Equations SI-1 through SI-4, from Han and Lawler (1992).

A curvilinear model was also presented as a set of corrections to the rectilinear collision frequency functions, following Han and Lawler (1992). These corrections account for hydrodynamic retardation and other short-range effects of particle collisions due to fluid motion. The correction factors applied to the rectilinear collision frequency functions, and the curvilinear total collision frequency are defined by Equations SI-5 through SI-8.

3. Results and Discussion

3.1. Effect on *M. aeruginosa* Cell Damage

Changes in FI were used to determine if IOM was released after the oxidation of *M. aeruginosa* cells with ferrate (Figure 1). The change in FI is represented by the difference between FI when Fe(VI) = 0 μM at some algal concentration and pH, and when Fe(VI) is added at the same conditions. Increases in FI indicate IOM release into the dissolved phase during oxidation, while decreases in FI correspond to IOM

release during oxidation, as well as further oxidation and compositional changes by Fe(VI) (Wert et al., 2014). FI detects released IOM by indicating the aromaticity of the organic matter (McKnight et al., 2001). Patterns in FI results were confirmed by results of UV_{254} absorbance (Figure SI-1) (Wert et al., 2014).

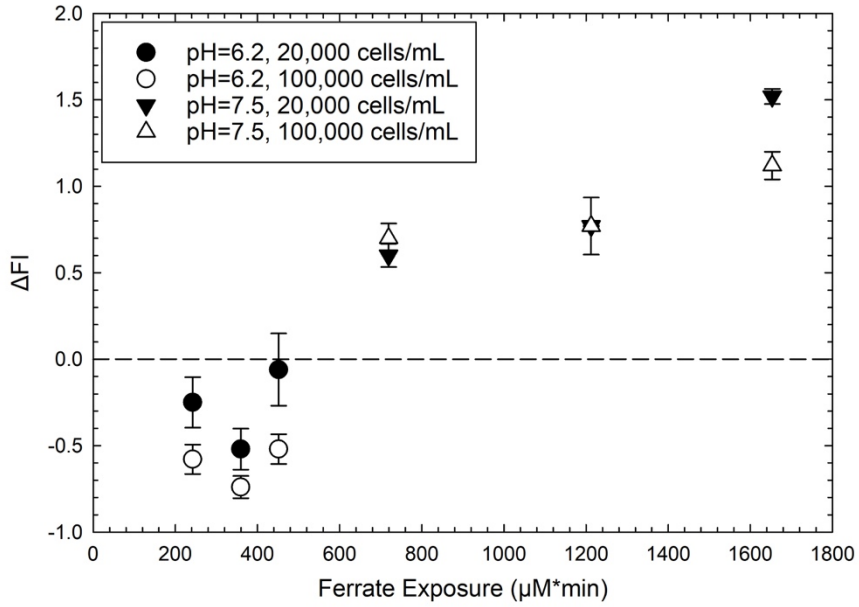

Figure 1. Changes in FI after oxidation of algal cells by ferrate in laboratory water matrix; 1 mM HCO_3^-, initial algal concentration ≈ 20,000 cells/mL or 100,000 cells/mL, pH = 6.2 or 7.5, Fe(VI) = 20, 50, or 100 μM. Each point represents the average change in FI of 3 measurements from when Fe(VI) = 0 μM. Error bars represent the positive and negative of one standard deviation.

At pH 6.2, all FI values are negative, indicating IOM release and further oxidation. The most significant decreases in FI at pH 6.2 occurred when the Fe(VI) dose was 50 μM (ferrate exposure = 359 μM•min) for both algal concentrations. When the pH was 7.5, a majority of the FI values were positive, which suggests that IOM was released during oxidation, but there was no further oxidation by Fe(VI). The largest increase in FI when pH = 7.5 occurred when Fe(VI) = 50 μM (ferrate exposure = 1212 μM•min) for the low algae concentration, but at Fe(VI) = 100 μM (ferrate exposure = 1653 μM•min) for

the high algae concentration. A comparison of the same *M. aeruginosa* concentrations and ferrate doses at differing pH values shows that IOM release and further oxidation occurs more frequently at pH 6.2.

It is noteworthy that IOM release and further oxidation was more prominent at a lower pH. At higher pH values, ferrate exposure is greater due to a slower Fe(VI) decay rate. However, Figure 1 shows more oxidation when the total exposure is less. This can be explained by the lower oxidation potential of ferrate at pH 7.5 versus 6.2 resulting from the dominance of $HFeO_4^-$ with larger oxo-ligand spin density then FeO_4^{-2} (pK_{a3} = 7.3) (Sharma, 2011). Figure 1 supports the conclusion that oxidation potential is more important than total oxidant exposure with respect to algal cell lysing. A similar pH dependence has been noted with respect to Fe(VI) transformation of DBP precursors (Jiang et al., 2016b). Utilities implementing Fe(VI) for HABs must focus on pH in addition to Fe(VI) dose.

Total nitrogen measurements (Figure SI-2) showed a decrease in TN concentrations with Fe(VI) dose after oxidation for all conditions, especially at pH 6.2, agreeing with FI results which may further support cell lysis. This signifies that nitrogen rich IOM is released and oxidized. In addition, many TN concentrations were below the detection limit (e.g. ~100% decrease), which suggests the limited formation of nitrogenated DBPs (N-DBPs) precursor material. However, even at low concentrations (i.e. $\leq$ 1 μM) certain N-DBPs (e.g. bromonitromethane) may still pose a chronic toxicity risk (Plewa et al., 2004). However, it is important to note that the relatively low TN values determined in this study it is difficult to see changes in TN values, meaning TN may not serve as an appropriate indirect method for quantifying cell lysis. A more in-depth discussion about the TN results can be found in Text SI-4.

Sphericity measurements (Figure 2 A & D) also show that cell lysing trends with Fe(VI) dose and pH. In general, the algal cells become less spherical when the Fe(VI) dose ranges from 20 to 50 μM, indicating that the integrity of the algal cells is compromised and lysing occurred. The decreased sphericity and deformed structure of lysed cells was confirmed visually using the 3-dimensional fluorescence images (Figure 2 C & F). Cells exposed to Fe(VI) have noticeable deformities and appear

less spherical compared to cells not exposed to Fe(VI) (Figure 2 B & E). Further discussion of the sphericity results are provided in Text SI-5.

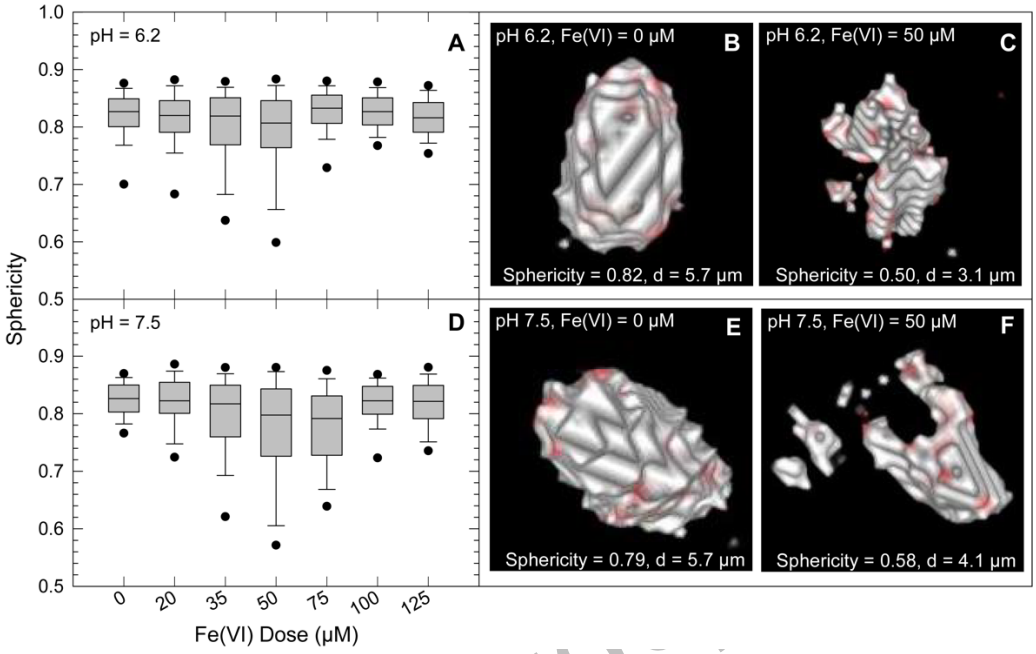

Figure 2: Sphericity trends of algal cells after oxidation with varying Fe(VI) dose at pH 6.2 and 7.5 (A & D). 3-dimensional confocal fluorescence images of individual algae cells before (B & E) and after (C & F) exposure to 50 µM Fe(VI) at pH 6.2 and 7.5, respectively. The images after exposure represent the most extreme cases of lysis (i.e. cell with lowest sphericity). Experimental conditions: 1 mM HCO_3^-, initial algal concentration ≈ 20,000 cells/mL. Each box and whisker plot represent the median, 10^{th}, 25^{th}, 75^{th}, and 90^{th} percentile of 3 cells. Each point represents the 5^{th} or 95^{th} percentile outlier. Detailed high-content phenotypic-screening confocal fluorescence microscopy instrumental methods are located in Text SI-3.

3.2. Effect on *M. aeruginosa* Surface Charge

Zeta potential values were measured to assess the stability of the colloidal suspension resulting from Fe(VI) pre-oxidation (Figure 3). A negative zeta potential corresponds to negative surface charges, and denotes incomplete destabilization (e.g. insufficient coagulation). A near-zero zeta potential signifies

negligible surface charges, and complete coagulation. The ZP values shown are a function of algal concentration, Fe(VI) dose, and pH.

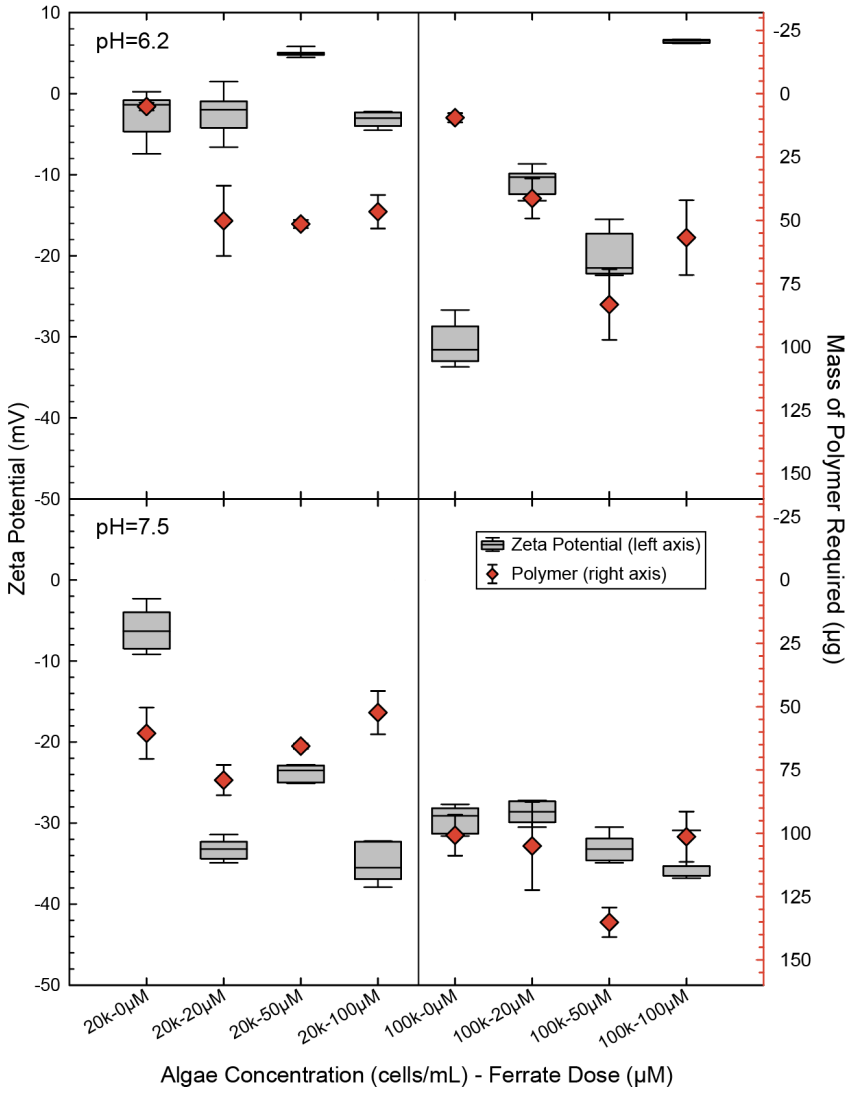

Figure 3. Zeta potential and mass of polymer required to reach a SCV of 0 for algal cells and ferrate particles after ferrate pre-oxidation in lab water matrix; 1 mM HCO_3^-, initial algal concentration ≈ 20,000 cells/mL or 100,000 cells/mL, pH = 6.2 or 7.5, Fe(VI) = 0, 20, 50, or 100 µM. Each box and whisker plot represents the median, 10th, 25th, 75th, and 90th percentile of 7 measurements. Each point represents the average of 2 charge titrations, with error bars representing the positive and negative of two standard deviations.

From Figure 3, less negative ZP values were observed at pH 6.2 than for pH 7.5. For example, at 20,000 cells/mL of algae and 50 μM of Fe(VI), the median ZP values at pH 6.2 and 7.5 were +4.93 mV and -23.5 mV. This outcome is in agreement with prior Fe(VI)-HAB system ZP results (Deng et al., 2017) and further implies that particle destabilization is accomplished by charge neutralization (Bernhardt and Clasen, 1991; Van Benschoten and Edzwald, 1990). Charge neutralization occurred at a lower pH because of the low zero point charge of *M. aeruginosa* (Bernhardt and Clasen, 1991; Pieterse and Cloot, 1997). There is also an increase in H+ ions at the lower pH, which serves to neutralize some sources of negative surface charge. When no Fe(VI) was added, near zero zeta potentials were recorded in the low algae condition. In general, increasing Fe(VI) doses lead to a less negative ZP at pH 6.2, and more negative ZP values when pH was 7.5 indicating incomplete coagulation occurred when the pH is greater than 7, and more complete coagulation occurred when the pH is 6.2. Therefore, pH plays an important role in the treatment process because it impacts Fe(VI) oxidation and surface charge.

Resulting colloidal suspensions were titrated with a cationic polymer to illustrate the extent of coagulation required after ferrate pre-oxidation (Figure 3). Titration curves indicating the amount of cationic polymer added over time versus the SCV are shown in Figure SI-4. The total amount of cationic polymer required to achieve a neutral charge during these titrations are presented in Figure 3. A larger amount of polymer required suggests incomplete coagulation after ferrate pre-oxidation. Fe(VI) alone may not be an adequate to fully destabilize an algal and Fe(III) particle suspension. A smaller mass of polymer required indicates a more neutral surface charge, and improved coagulation performance. In general, the titration results trend with zeta potentials (Barron et al., 1994). In the cases where this is not true, the discrepancies can be attributed to differences between the analytical approaches. The DLS technique optically measures the electrophoretic mobility of particles only < 10 μm in order to calculate ZP. On the other hand, the LCA imparts motion to the suspension in order shear layer surface charges. The displaced ions then create a current with a magnitude corresponding to the amount of charge on the particles.

More polymer was required when the pH was 7.5 than for the same conditions at pH 6.2. For instance, when the algal concentration is 100,000 cells/mL and Fe(VI) = 50 μM, the required mass of polymer for pH 6.2 and 7.5 is 83 μg and 135 μg respectively. Overall, the addition of Fe(VI) did not obviate the need for downstream coagulation, as assessed by the LCA. More polymer was required after Fe(VI) was added to allow van der Waals forces to govern, and to destabilize the particles. This is more evident at pH 6.2. The increase in the amount of polymer required is likely due to the increase in the total number of particles and concentration of surfaces on a μm^2/mL basis from Fe(VI), and the limited formation of positively charged iron-hydrolysis products from ferrate resultant iron (Deng et al., 2018; Goodwill et al., 2015; Lv et al., 2018).

The surface charge of the ferrate resultant particles and algae system was also impacted by cell lysing. As the algal cells are lysed, IOM is released. IOM mainly consists of proteins, polysaccharides, and lipids (Brown et al., 1997; Pivokonsky et al., 2006) that behave as anionic and non-ionic polyelectrolytes (Bernhardt and Clasen, 1991; Ma et al., 2012b), and thus can hinder aggregation, resulting is more cationic polymer required for particle destabilization (Chen and Yeh, 2005; Plummer and Edzwald, 2002). The surface charge as assessed by ZP trended with the evidence of lysing depicted in Figure 1 and Figure SI-3. The most negative changes in FI correspond to the near zero and positive zeta potentials, while the most positive changes in FI correspond to the most negative zeta values. From these results, Fe(VI)-induced IOM release is an important factor in coagulation within the algae-Fe(VI) system. When IOM is released, zeta potentials become more negative due to the negative charge of released IOM. Conversely, release of IOM followed by subsequent oxidation, which only occurred at pH 6.2, yields less negative ZP values. This agrees with previous research that stated *M. aeruginosa* cells are increasingly negatively charged with increasing pH (Hadjoudja et al., 2010). The addition of cationic polymer after pre-oxidation was always necessary to achieve a SCV of 0 on the LCA; however, some zeta potential values were positive for instances where the SCV was not 0. Different full-scale operations have different protocols for determining their basis for sufficient coagulation. For instance, a SCV of 0 is not necessarily

required for acceptable coagulation at the full-scale. In the majority of experimental conditions, Fe(VI) alone may be inadequate for both oxidation and coagulation processes at the pH values chosen. However, decreasing the pH below 6.2 could allow the Fe(VI)-algae system to become less stable, or more conducive to aggregation. The addition of acid and ferrate together as an advanced oxidation process has recently been explored (Manoli et al., 2017). Hydrolyzing metal salt coagulants will also decrease pH.

3.3. Effect on Collision Frequency

Figure 4 illustrates the rate of rectilinear and curvilinear collisions between a Fe(VI) and algal particle for a range of incident particle diameters and two particle densities after oxidation of 100,000 cells/mL of algae by 50 μM of Fe(VI). The x-axis denotes the particle size diameter of the particle colliding with an average size Fe(VI)-algae particle (9.38 μm). The y-axis represents the rate of collisions for each particle size pair per cm^3/s, for each collision mechanism (Brownian motion – β_{μ}, fluid shear – β_M, differential sedimentation – β_{DS}, and total – β_{ij}). The curvilinear models differ from the rectilinear in that they apply a set of correction factors that account for hydrodynamic retardation and other short-range effects in particle collisions due to mixing (Han and Lawler, 1992). The dominant mode of collision is defined as the top line closest to the total collision frequency function for a certain range of particle sizes.

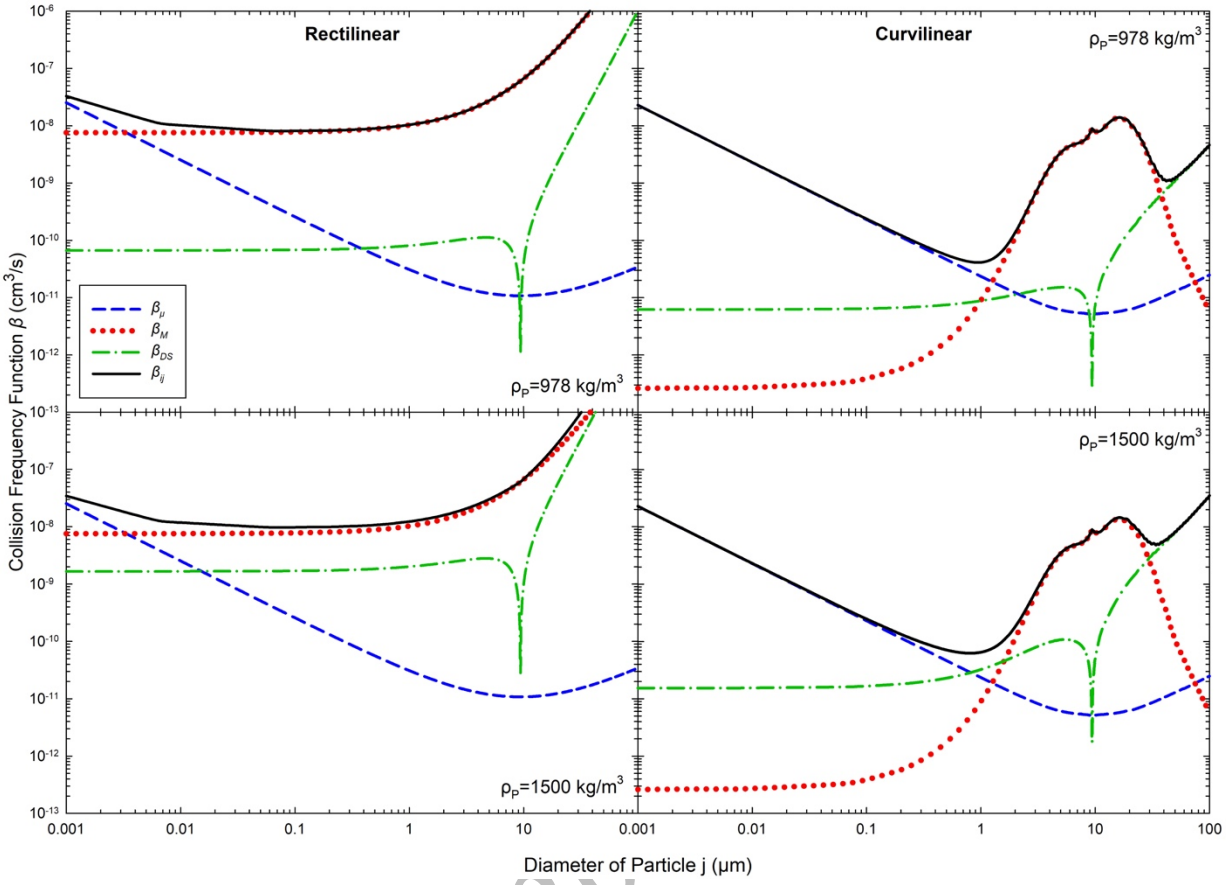

Figure 4. Collision frequency functions after oxidation of algal cells by ferrate in lab water matrix; 1 mM HCO_3^-, initial algal concentration ≈ 100,000 cells/mL, Fe(VI) = 50 µM. Each line represents a rectilinear or curvilinear collision frequency function occurring due to β_μ, β_M, β_{DS}, or β_{ij} over different diameters of particle j. Experimental conditions: d_i = 9.38 µm, ρ_P = 978 kg/m^3, or 1500 kg/m^3, T = 20°C, G = 55 s^{-1}.

For the rectilinear model, when ρ_P = 978 kg/m^3, Brownian motion dominates only when one particle diameter is very small (< 0.005 µm). When the particle size is ≥ 0.005 µm, fluid shear, or mixing, becomes the dominant coagulation mechanism, and differential settling never dominates. When the particle density is increased, β_μ is again dominant only when one particle diameter is very small (< 0.005 µm). However, the particle size range in which β_M is the dominant coagulation mechanism decreases to between 0.005 µm and 52 µm. Differential settling is then dominant when the incident particle is very large (> 52 µm). The rectilinear model predicts fluid shear as the dominate mechanism for most collisions

in the Fe(VI)-algae suspension. This is also true for varying algal concentrations, pH values, and Fe(VI) doses (Figure SI-5 and Figure SI-6).

For the curvilinear models, Brownian motion dominants over an additional three orders of magnitude compared to the rectilinear model, regardless of particle density (< 1.3 μm and < 0.9 μm). The range in which mixing dominates decreases to when particles are about 1 to 30 μm, allowing β_{DS} to dominant over a larger range of particle diameters (> 30 μm). This decreased importance of the mixing collision mechanism is the primary outcome of the curvilinear model (Han and Lawler, 1992).

A prior study conducted by Lv et al. (2018) concluded that sweep flocculation is the dominant collision mechanism in an ferrate system, based on typical coagulation process operating ranges developed by Amirtharajah and Mills (1982). However, this analysis did not consider the rate of differential setting and the hydrodynamic retardation and other short-range effects of particle collisions. Differential setting is a key component of sweep flocculation, and may be uniquely impacted by high number concentrations of algal particles with relative low density and corresponding settling velocities. The modeling results in Figure 4 demonstrate that β_{DS} is a dominate collision mechanism only when particles are quite large and relatively dense. Particle suspension results from Fe(VI) pre-oxidation of *M. aeruginosa* are polydisperse, and include significant contributions in the 0.1 to 10 μm size range (see Figure 5). Therefore, the modeling results from Figure 4 indicate that fluid shear, not differential settling, is the important collision mechanism in the case of ferrate resultant particles colliding with *M. aeruginosa* cells. The importance of mixing for particle collisions will warrant attention to flocculation practices when using Fe(VI) for HABs.

3.4. Particle Size

Figure 5 shows the number particle size distribution counted by the DLS and LLB particle counter after ferrate oxidation for a particle size range from 0.01 to 100 μm, for an initial algal concentration of 100,000 cells/mL and 0, 20, 50, or 100 μM of Fe(VI). The left y-axis displays the percent of the number of particles at a specific diameter counted by the DLS instrument, while the right y-axis displays the

percent counted by the LLB particle counter. Figure SI-7 depicts a similar set of results, but for an initial concentration of 20,000 cells/mL of algae.

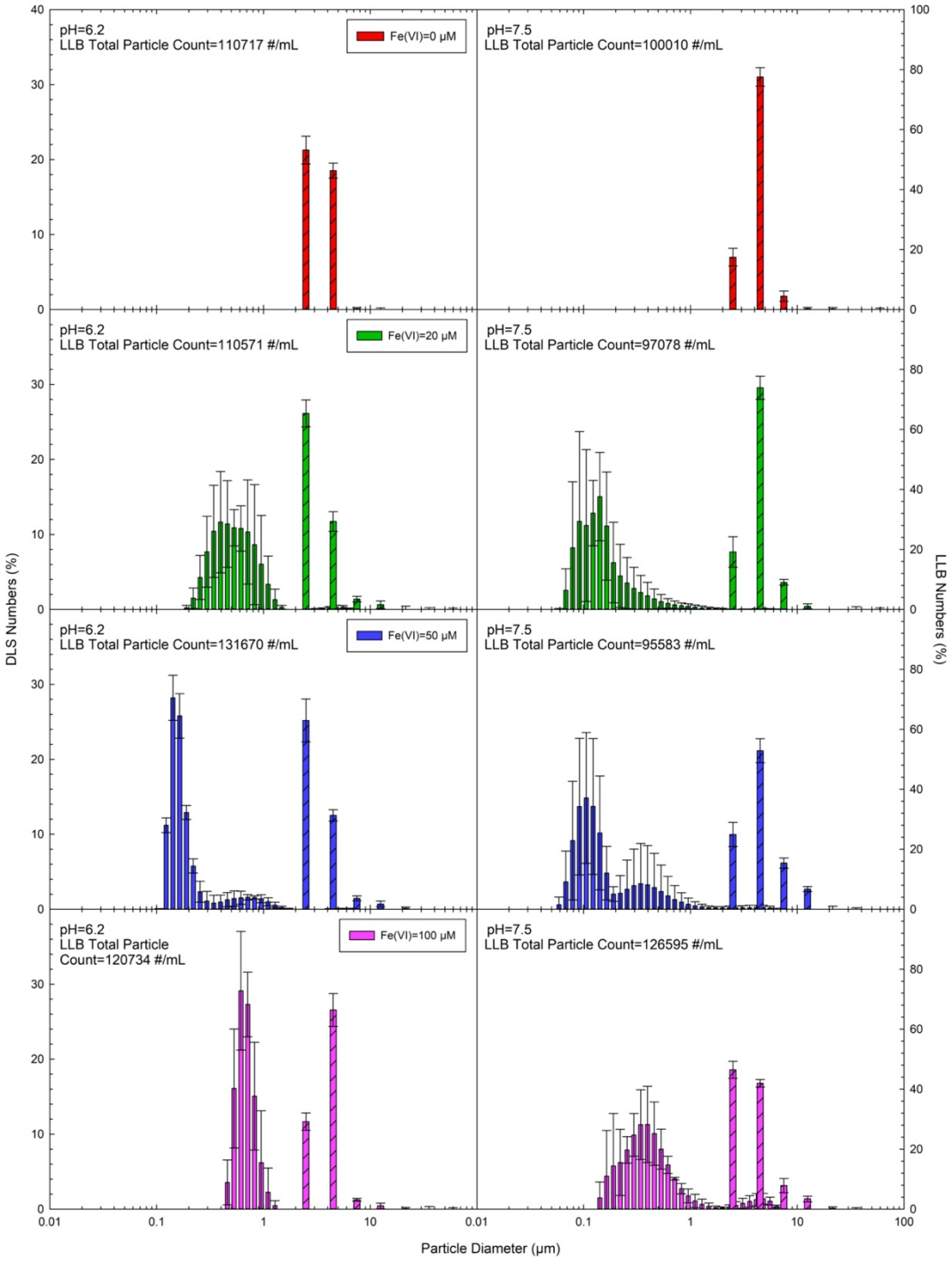

Figure 5. Number particle size distribution counted by the DLS and LLB particle counter for algal cells and ferrate particles after ferrate pre-oxidation in laboratory water matrix; 1 mM HCO_3^-, initial algal

concentration ≈ 100,000 cells/mL, pH = 6.2 or 7.5, Fe(VI) = 0, 20, 50, or 100 μM. Each unhatched bar represents the mean of 7 measurements conducted by the DLS, counted in predefined size channels with error bars representing the positive and negative of one standard deviation. Each hatched bar represents the mean of 3 measurements conducted by the LLB particle counter, counted in predefined size channels with error bars representing the positive and negative of one standard deviation.

From the DLS data in Figure 5, an increase in particle size occurred with increasing Fe(VI) doses for both pH values, indicating aggregation. In addition, the increase in particle sizes is more pronounced at pH 6.2 than 7.5, consistent with surface charge analysis. The DLS approach also shows that at pH 6.2, almost all of the particles are larger than 200 nm, while at pH 7.5, a significant number of particles are less than 100 nm. A lower algal concentration yielded similar particle size results (Figure SI-7). The largest average particle size when algae = 20,000 cells/mL and 100,000 cells/mL occurred when Fe(VI) = 50 μM and 100 μM. This implies that more ferrate is required for similar levels of aggregation as the algal concentration increases.

The PSDs from the LLB particle counter show that approximately 98% of particles counted had a diameter between 2 and 10 μm, however, larger flocs were visually observed. These larger flocs likely exceeded the upper limit of the LLB instrument (125 μm). Particle distributions in this size range changes slightly as a result of Fe(VI). At pH 6.2, particle sizes increased by ~1.0 μm on average after Fe(VI) was added, while at pH 7.5, particle sizes only increased by 0.13 μm on average. LLB results support better coagulation performance at pH 6.2. Again, the lower algal concentration produced comparable results (Figure SI-7). A decrease in the total number of particles after pre-oxidation was measured likely due to the formation of flocs > 125 μm. Iron fraction results show almost all Fe was operationally-defined as large (Figure SI-8). However, based on the PSDs, there are a significant number of particles < 10 μm. This confirms that Brownian motion and mixing play an important role in collisions between resultant particles.

4. Conclusions

- Fe(VI) lyses algal cells at conditions relevant to common HABs in drinking water supply, and may serve as a novel, low capital-expenditure on-demand treatment approach to periodic HABs.
- Lysing and subsequent oxidation of AOM were a strong function of pH, not the overall Fe(VI) exposure (e.g. contact time). However, lysis and AOM oxidation would likely decrease in the presence of NOM.
- Fe(VI) pre-oxidation is capable of decreasing TN concentrations by subsequent oxidation of released IOM.
- Complete coagulation in the Fe(VI)-algae system is likely not occurring. Additional polymer is required in all cases to achieve a SCV of 0. However, a system at pH 6.2 is more conducive for coagulation than at pH 7.5.
- Fluid-shear is an important particle collision mechanism in the Fe(VI)-algae system.
- Fe(VI) increased resultant particle sizes. Resulting suspensions were polydisperse. In all cases, particle size increased with the addition of Fe(VI). However, the shift was more pronounced when pH was 6.2. A majority of the particles by mass were large.

Acknowledgements

This research was funded by the Rhode Island Water Resources Center (Director: Leon T. Thiem, P.E., Ph.D). The funding agency was not involved in any aspect of this research or reporting and all views expressed in this manuscript belong solely to the authors. The authors thank Element 26 Technology (League City, TX; soundar.ramchandran@gmail.com; jtstrehl@gmail.com) for supplying potassium ferrate product for this study. The authors acknowledge Ashley Bair and Christopher M. Miller, P.E., Ph.D. (Fontus Blue, Akron, OH) for assistance preparing and growing algal cultures. The Opera Phenix high-content screening system was purchased through the National Science Foundation Major Research Instrumentation grant #1828057.

Appendix A. Supplementary Data

Supplementary data to this article can be found online.

References

Alshahri, A.H., Fortunato, L., Ghaffour, N., Leiknes, T., 2019. Advanced coagulation using in-situ generated liquid ferrate, Fe (VI), for enhanced pretreatment in seawater RO desalination during algal blooms. Sci. Total Environ. 685, 1193–1200. https://doi.org/10.1016/j.scitotenv.2019.06.286

Amirtharajah, A.A., Mills, K.M., 1982. Rapid-mix design for mechanisms of alum coagulation. Am. Water Work. Assoc. 74, 210–216.

Anderson, L.E., Krkošek, W.H., Stoddart, A.K., Trueman, B.F., Gagnon, G.A., 2017. Lake Recovery Through Reduced Sulfate Deposition: A New Paradigm for Drinking Water Treatment. Environ. Sci. Technol. 51, 1414–1422. https://doi.org/10.1021/acs.est.6b04889

Bache, D.H., Gregory, R., 2010. Flocs and separation processes in drinking water treatment: a review. J. Water Supply Res. Technol. 59, 16–30. https://doi.org/10.2166/aqua.2010.028

Barron, W., Murray, B.S., Scales, P.J., Healy, T.W., Dixon, D.R., Pascoe, M., 1994. The streaming current detector: A comparison with conventional electrokinetic techniques. Colloids Surfaces A Physicochem. Eng. Asp. 88, 129–139. https://doi.org/10.1016/0927-7757(94)02824-9

Bernhardt, H., Clasen, J., 1991. Flocculation of micro-organisms. J. Water Supply Res. Technol. 40, 76–87.

Bouchard, M.F., Surette, C., Cormier, P., Foucher, D., 2018. Low level exposure to manganese from drinking water and cognition in school-age children. Neurotoxicology 64, 110–117. https://doi.org/10.1016/j.neuro.2017.07.024

Brooks, B.W., Lazorchak, J.M., Howard, M.D.A., Johnson, M.-V. V., Morton, S.L., Perkins, D.A.K., Reavie, E.D., Scott, G.I., Smith, S.A., Steevens, J.A., 2016. Are harmful algal blooms becoming the

448 greatest inland water quality threat to public health and aquatic ecosystems? Environ. Toxicol.
449 Chem. 35, 6–13. https://doi.org/10.1002/etc.3220

450 Brown, M.R., Jeffrey, S.W., Volkman, J.K., Dunstan, G.., 1997. Nutritional properties of microalgae for
451 mariculture. Aquaculture 151, 315–331. https://doi.org/10.1016/S0044-8486(96)01501-3

452 Chandrakanth, M.S., Amy, G.L., 1996. Effects of Ozone on the Colloidal Stability and Aggregation of
453 Particles Coated with Natural Organic Matter. Environ. Sci. Technol. 30, 431–443.
454 https://doi.org/10.1021/es9500567

455 Chen, J.J., Yeh, H.H., 2005. The mechanisms of potassium permanganate on algae removal. Water Res.
456 39, 4420–4428. https://doi.org/10.1016/j.watres.2005.08.032

457 Codd, G.A., Bell, S.G., Brooks, W.P., 1989. Cyanobacterial Toxins in Water. Water Sci. Technol. 21, 1–
458 13. https://doi.org/10.2166/wst.1989.0071

459 Cory, R.M., Miller, M.P., McKnight, D.M., Guerard, J.J., Miller, P.L., 2010. Effect of instrument-specific
460 response on the analysis of fulvic acid fluorescence spectra. Limnol. Oceanogr. Methods 8, 67–78.
461 https://doi.org/10.4319/lom.2010.8.67

462 Cui, J., Zheng, L., Deng, Y., 2018. Emergency water treatment with ferrate(<scp>vi</scp>) in response
463 to natural disasters. Environ. Sci. Water Res. Technol. 4, 359–368.
464 https://doi.org/10.1039/C7EW00467B

465 Dang, T.C., Fujii, M., Rose, A.L., Bligh, M., Waite, T.D., 2012. Characteristics of the Freshwater
466 Cyanobacterium Microcystis aeruginosa Grown in Iron-Limited Continuous Culture. Appl. Environ.
467 Microbiol. 78, 1574–1583. https://doi.org/10.1128/AEM.06908-11

468 DeLuca, S.J., Chao, A.C., Smallwood, C., 1983. Ames Test of Ferrate Treated Water. J. Environ. Eng.
469 109, 1159–1167. https://doi.org/10.1061/(ASCE)0733-9372(1983)109:5(1159)

470 Deng, Y., Jung, C., Liang, Y., Goodey, N., Waite, T.D., 2018. Ferrate(VI) decomposition in water in the

absence and presence of natural organic matter (NOM). Chem. Eng. J. 334, 2335–2342. https://doi.org/10.1016/j.cej.2017.12.006

Deng, Y., Wu, M., Zhang, H., Zheng, L., Acosta, Y., Hsu, T.T.D., 2017. Addressing harmful algal blooms (HABs) impacts with ferrate(VI): Simultaneous removal of algal cells and toxins for drinking water treatment. Chemosphere. https://doi.org/10.1016/j.chemosphere.2017.08.052

Drikas, M., Chow, C.W.K., House, J., Burch, M.D., 2001. Using Coagulation, Flocculation, and Settling to Remove Toxic cyanobacteria. J. Am. Water Works Assoc. 93, 100–111. https://doi.org/10.1002/j.1551-8833.2001.tb09130.x

Fan, J., Lin, B.-H., Chang, C.-W., Zhang, Y., Lin, T.-F., 2018. Evaluation of potassium ferrate as an alternative disinfectant on cyanobacteria inactivation and associated toxin fate in various waters. Water Res. 129, 199–207. https://doi.org/10.1016/j.watres.2017.11.026

Fang, J., Ma, J., Yang, X., Shang, C., 2010. Formation of carbonaceous and nitrogenous disinfection by-products from the chlorination of Microcystis aeruginosa. Water Res. 44, 1934–1940. https://doi.org/10.1016/j.watres.2009.11.046

Gan, W., Sharma, V.K., Zhang, X., Yang, L., Yang, X., 2015. Investigation of disinfection byproducts formation in ferrate(VI) pre-oxidation of NOM and its model compounds followed by chlorination. J. Hazard. Mater. 292, 197–204. https://doi.org/10.1016/j.jhazmat.2015.02.037

Goodwill, J.E., Jiang, Y., Reckhow, D.A., Gikonyo, J., Tobiason, J.E., 2015. Characterization of particles from ferrate preoxidation. Environ. Sci. Technol. 49, 4955–4962. https://doi.org/10.1021/acs.est.5b00225

Hadjoudja, S., Deluchat, V., Baudu, M., 2010. Cell surface characterisation of Microcystis aeruginosa and Chlorella vulgaris. J. Colloid Interface Sci. 342, 293–299. https://doi.org/10.1016/j.jcis.2009.10.078

Han, M., Lawler, D.F., 1992. (Relative) insignificance of G in flocculation. J. / Am. Water Work. Assoc.

84, 79–91. https://doi.org/10.1002/j.1551-8833.1992.tb05869.x

Huang, X., Deng, Y., Liu, S., Song, Y., Li, N., Zhou, J., 2016. Formation of bromate during ferrate(VI) oxidation of bromide in water. Chemosphere 155, 528–533. https://doi.org/10.1016/j.chemosphere.2016.04.093

Jiang, W., Chen, L., Batchu, S.R., Gardinali, P.R., Jasa, L., Marsalek, B., Zboril, R., Dionysiou, D.D., O'Shea, K.E., Sharma, V.K., 2014. Oxidation of Microcystin-LR by Ferrate(VI): Kinetics, Degradation Pathways, and Toxicity Assessments. Environ. Sci. Technol. 48, 12164–12172. https://doi.org/10.1021/es5030355

Jiang, Y., Goodwill, J.E., Tobiason, J.E., Reckhow, D.A., 2019. Comparison of ferrate and ozone pre-oxidation on disinfection byproduct formation from chlorination and chloramination. Water Res. 156, 110–124. https://doi.org/10.1016/j.watres.2019.02.051

Jiang, Y., Goodwill, J.E., Tobiason, J.E., Reckhow, D.A., 2016a. Bromide oxidation by ferrate(VI): The formation of active bromine and bromate. Water Res. 96, 188–197. https://doi.org/10.1016/j.watres.2016.03.065

Jiang, Y., Goodwill, J.E., Tobiason, J.E., Reckhow, D.A., 2016b. Impacts of ferrate oxidation on natural organic matter and disinfection byproduct precursors. Water Res. 96, 114–125. https://doi.org/10.1016/j.watres.2016.03.052

Kenefick, S.L., Hrudey, S.E., Peterson, H.G., Prepas, E.E., 1993. Toxin Release from Microcystis Aeruginosa after Chemical Treatment. Water Sci. Technol. 27, 433–440. https://doi.org/10.2166/wst.1993.0387

Lee, Y., Yoon, J., Von Gunten, U., 2005. Spectrophotometric determination of ferrate (Fe(VI)) in water by ABTS. Water Res. 39, 1946–1953. https://doi.org/10.1016/j.watres.2005.03.005

Li, M., Zhu, W., Guo, L., Hu, J., Chen, H., Xiao, M., 2016. To increase size or decrease density?

Different Microcystis species has different choice to form blooms. Sci. Rep. 6, 37056. https://doi.org/10.1038/srep37056

Liu, S., Xu, J., Chen, W., David, B.E., Wu, M., Ma, F., 2017. Impacts of potassium ferrate(VI) on the growth and organic matter accumulation, production, and structural changes in the cyanobacterium Microcystis aeruginosa. Environ. Sci. Pollut. Res. 24, 11299–11308. https://doi.org/10.1007/s11356-017-8757-3

Liu, W., Liang, Y.-M., 2008. Use of Ferrate(VI) in Enhancing the Coagulation of Algae-Bearing Water: Effect and Mechanism Study, in: ACS Symposium Series. pp. 434–445. https://doi.org/10.1021/bk-2008-0985.ch027

Loganathan, K., 2016. Ozone-based advanced oxidation processes for the removal of harmful algal bloom (HAB) toxins: a review. Desalin. WATER Treat. 59, 65–71. https://doi.org/10.5004/dwt.2016.0346

Lv, D., Zheng, L., Zhang, H., Deng, Y., 2018. Coagulation of colloidal particles with ferrate(VI). Environ. Sci. Water Res. Technol. 4, 701–710. https://doi.org/10.1039/C8EW00048D

Ma, J., Liu, W., 2002. Effectiveness and mechanism of potassium ferrate(VI) preoxidation for algae removal by coagulation. Water Res. 36, 871–878. https://doi.org/10.1016/S0043-1354(01)00282-2

Ma, M., Liu, R., Liu, H., Qu, J., 2012a. Effect of moderate pre-oxidation on the removal of Microcystis aeruginosa by KMnO4–Fe(II) process: Significance of the in-situ formed Fe(III). Water Res. 46, 73–81. https://doi.org/10.1016/j.watres.2011.10.022

Ma, M., Liu, R., Liu, H., Qu, J., Jefferson, W., 2012b. Effects and mechanisms of pre-chlorination on Microcystis aeruginosa removal by alum coagulation: Significance of the released intracellular organic matter. Sep. Purif. Technol. 86, 19–25. https://doi.org/10.1016/j.seppur.2011.10.015

Manoli, K., Nakhla, G., Ray, A.K., Sharma, V.K., 2017. Oxidation of caffeine by acid-activated ferrate(VI): Effect of ions and natural organic matter. AIChE J. 63, 4998–5006.

https://doi.org/10.1002/aic.15878

McKnight, D.M., Boyer, E.W., Westerhoff, P.K., Doran, P.T., Kulbe, T., Andersen, D.T., 2001. Spectrofluorometric characterization of dissolved organic matter for indication of precursor organic material and aromaticity. Limnol. Oceanogr. 46, 38–48. https://doi.org/10.4319/lo.2001.46.1.0038

Monzyk, I.B.F., Creek, T., Smeltz, A.D., Rose, J.K., 2013. Method for producing ferrate (V) and/or (VI). US 8.449,756 B2.

Paerl, H.W., Huisman, J., 2008. CLIMATE: Blooms Like It Hot. Science (80-.). 320, 57–58. https://doi.org/10.1126/science.1155398

Pieterse, A.J.H., Cloot, A., 1997. Algal cells and coagulation, flocculation and sedimentation processes. Water Sci. Technol. 36, 111–118.

Pivokonsky, M., Kloucek, O., Pivokonska, L., 2006. Evaluation of the production, composition and aluminum and iron complexation of algogenic organic matter. Water Res. 40, 3045–3052. https://doi.org/10.1016/j.watres.2006.06.028

Plewa, M.J., Wagner, E.D., Jazwierska, P., Richardson, S.D., Chen, P.H., McKague, A.B., 2004. Halonitromethane Drinking Water Disinfection Byproducts: Chemical Characterization and Mammalian Cell Cytotoxicity and Genotoxicity. Environ. Sci. Technol. 38, 62–68. https://doi.org/10.1021/es030477l

Plummer, J.D., Edzwald, J.K., 2002. Effects of chlorine and ozone on algal cell properties and removal of algae by coagulation. J. Water Supply Res. Technol. 51, 307–318. https://doi.org/10.2166/aqua.2002.0027

Prucek, R., Tuček, J., Kolařík, J., Filip, J., Marušák, Z., Sharma, V.K., Zbořil, R., 2013. Ferrate(VI)-induced arsenite and arsenate removal by in situ structural incorporation into magnetic iron(III) oxide nanoparticles. Environ. Sci. Technol. 47, 3283–3292. https://doi.org/10.1021/es3042719

563 Rice, E.W., Baird, R.B., Eaton, A.D., Clesceri, L.S. (Eds.), 2012. Standard Methods For the Examination
564 of Water and Wastewater, 22nd ed. APHA, AWWA, and WEF, Washington, DC.

565 Sharma, V.K., 2011. Oxidation of inorganic contaminants by ferrates (VI, V, and IV)–kinetics and
566 mechanisms: A review. J. Environ. Manage. 92, 1051–1073.
567 https://doi.org/10.1016/j.jenvman.2010.11.026

568 Sharma, V.K., Chen, L., Zboril, R., 2016. Review on High Valent FeVI(Ferrate): A Sustainable Green
569 Oxidant in Organic Chemistry and Transformation of Pharmaceuticals. ACS Sustain. Chem. Eng. 4,
570 18–34. https://doi.org/10.1021/acssuschemeng.5b01202

571 Sharma, V.K., Zboril, R., Varma, R.S., 2015. Ferrates: Greener Oxidants with Multimodal Action in
572 Water Treatment Technologies. Acc. Chem. Res. 48, 182–191. https://doi.org/10.1021/ar5004219

573 Tobiason, J.E., Bazilio, A., Goodwill, J., Mai, X., Nguyen, C., 2016. Manganese Removal from Drinking
574 Water Sources. Curr. Pollut. Reports 2, 168–177. https://doi.org/10.1007/s40726-016-0036-2

575 Van Benschoten, J.E., Edzwald, J.K., 1990. Chemical Aspects of Coagulation Using Aluminum Salts I-
576 Hydrolytic Reactions of Alum and Polyaluminum Chloride. Water Res. 24, 1519–1526.

577 Vlaski, A., 1998. Microcystic Aeruginosa Removal Air Flotation (DAF) Options for Enhanced Process
578 Operation and Kinetic Modelling. Delft University of Technology.

579 Wert, E.C., Korak, J.A., Trenholm, R.A., Rosario-Ortiz, F.L., 2014. Effect of oxidant exposure on the
580 release of intracellular microcystin, MIB, and geosmin from three cyanobacteria species. Water Res.
581 52, 251–259. https://doi.org/10.1016/j.watres.2013.11.001

582 WHO, 2003. Guidelines for safe recreational water environments.

583 Xie, P., Ma, J., Fang, J., Guan, Y., Yue, S., Li, X., Chen, L., 2013. Comparison of Permanganate
584 Preoxidation and Preozonation on Algae Containing Water: Cell Integrity, Characteristics, and
585 Chlorinated Disinfection Byproduct Formation. Environ. Sci. Technol. 47, 14051–14061.

https://doi.org/10.1021/es4027024

Yuan, B.-L., Qu, J.-H., Fu, M.-L., 2002. Removal of cyanobacterial microcystin-LR by ferrate oxidation–coagulation. Toxicon 40, 1129–1134. https://doi.org/10.1016/S0041-0101(02)00112-5

Zhou, S., Shao, Y., Gao, N., Zhu, S., Li, L., Deng, J., Zhu, M., 2014. Removal of Microcystis aeruginosa by potassium ferrate (VI): Impacts on cells integrity, intracellular organic matter release and disinfection by-products formation. Chem. Eng. J. 251, 304–309. https://doi.org/10.1016/j.cej.2014.04.081